



20th IAHR International Symposium on Ice
Lahti, Finland, June 14 to 18, 2010

Modeling Lake Erie ice dynamics: Process studies

Jia Wang¹, Haoguo Hu², and Xuezhi Bai²

¹*NOAA Great Lakes Environmental Research Laboratory
4840 S. State Road, Ann Arbor, MI 48108; Email: jia.wang@noaa.gov; Tel:
734-741-2281*

²*Cooperative Institute for Limnology and Ecosystems Research, University of Michigan
4840 S. State Road, Ann Arbor, MI 48108*

Abstract. A Great Lakes Ice-circulation Model (GLIM) with a 2-km resolution grid was applied to Lake Erie under hourly high-frequency atmospheric forcing derived from meteorological measurements. After the seasonal cycles of ice concentration, thickness, velocity, and other variables were well reproduced in the 2003/04 ice season in comparison with satellite measurements, process studies were further conducted on ice dynamics. Categories of ice thickness and ice speed were further investigated using available ice drifting measurements. The simulated ice velocity speeds resemble some important features of the observed ice drifts.

1. Introduction

Lake Erie (Fig.1) ice is first year ice, with ice thickness being typically a few centimeters to one meter or more due to ice ridging or rafting caused by wind and waves. Synoptic weather patterns and cyclone passage (Lofgren and Bleniek, 2008) can significantly affect lake ice distribution. Thus, numerical ice modelling is an important tool (Wang et al. 2010a) to help understand lake ice thermodynamic and dynamic features on synoptic time scales because predictability of lake ice using statistical methods is poor due to the complexity of the climate patterns (Assel and Rodionov, 1998; Mysak et al., 1996; Wang et al. 2010b) and highly dynamic regional weather patterns.

There were early initial efforts in the development of ice only modeling in Lake Erie (Wake and Rumer, 1979, 1983) based on Hibler's (1979) dynamic-thermodynamic sea-ice model; however, no substantial progress has been made over the last three decades. Recently, Wang et al. (2010a) developed a Coupled Great Lakes Ice-circulation Model (GLIM) to simulate a seasonal cycle of Lake Erie ice for use as a research and operational forecast tool. There have been some successful efforts in coupled ice-ocean modeling in many subpolar seas and bays, such as in Hudson Bay (Wang et al., 1994; Saucier and Dionne, 1998; Saucier et al., 2004), in the Gulf of St. Lawrence (Saucier et al., 2003), in the Baltic Sea (Meier et al., 2002 a, b; Haapala, 2000; Haapala et al., 2001), and in the Labrador Sea (Yao et al., 2000; Tang 2008). These areas are similar (except for salinity) to the Great Lakes because they do not have perennial ice cover.

The capability of modeling lake ice over a winter is crucial to many ice-related research and activities. Without an ice model, lake hydrodynamic models and wave models to forecast wave height must be empirically treated when ice cover exists. However, ecosystem models cannot be run over a winter without an ice model. Increasing needs for predicting lake ice for navigation, weather forecasting, rescue efforts, and ecosystem studies also motivated us to develop ice-circulation models. Based on our previous development of GLIM (Wang et al. 2010a), lake ice processes are further investigated in this study using ice drifting data and satellite measurements.

2. Model and Atmospheric Forcing

The GLIM is a combination of a Coupled Ice-Ocean Model (CIOM) developed and applied to the Arctic Ocean and subpolar seas (Yao et al., 2000; Wang et al., 2002, 2005,

2008, 2009) and the Great Lakes version of the Princeton Ocean Model (POM, Wang et al. 2010a). The CIOM is based on a thermodynamic and a dynamic model with a viscous-plastic sea ice constitutive law (Hibler, 1979) and a multi-category ice thickness distribution function (Thorndike et al., 1975; Hibler, 1980), coupled to the Princeton Ocean Model. The coupling is governed by the boundary processes as discussed by Mellor and Kantha (1989). The GLIM was described in detail and successfully applied to Lake Erie (Wang et al. 2010a). Table 1 lists the parameters used in the GLIM.

The GLIM was initialized with a uniform water temperature of 2°C on April 1, 2003, while salinity was set to zero. Initial ice concentration, thickness, and velocity were set to zero. The model was run from April 1, 2003 to December 31, 2004 using measured hourly atmospheric forcings derived from the coastal and airport stations (Fig. 1).

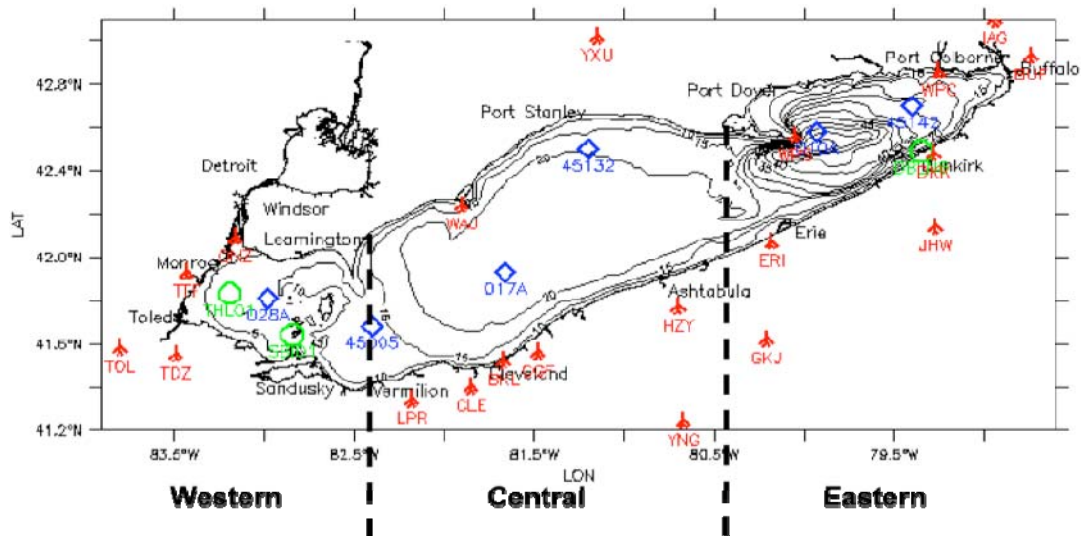


Figure 1. Lake Erie bathymetry (depths are in meters) and the model domain with 2-km resolution. The meteorological forcing of the model is derived from the NDBC (National Data Buoy Center) buoys (\diamond /blue), C-Man (Coastal Marine Automatic Network) stations (\circ /green), and local airports (red). The vertical dashed lines (82.4W and 80.4W) divide Lake Erie into the western, central, and eastern basins.

3. Process Studies

3.1 Seasonal cycle of temporal and spatial variability

Lake ice area is defined as the product of the grid area and ice concentration (Wang et al., 1994). Wang et al. (2010a) has successfully simulated the 2003-2004 ice season (see their Fig. 3) from December 1, 2003 to April 30, 2004, which is reproduced here (Fig.

2). The model simulation of the seasonal cycle compares reasonably well to the satellite-derived ice area. Lake ice started to form in December 2003, and slowly grew. Lake ice rapidly grew in January, reached a maximum around January 20, 2004 and persisted until mid-February. Lake ice suddenly retreated on February 22, because of a warming event due to a cyclone passage (see Fig. 2a), which has been discussed in detail in Wang et al. (2010a). Beginning in March, lake ice rapidly decreased because two warming events persisted throughout March. Lake ice was completely melted by mid-April. There is some discrepancy between the simulation and the measurements with mean bias deviation (MBD) being 7.4% and root mean square deviation (RMSD) being 1,840 km². The model produces more ice than was observed from late January to early February, and less ice in late March (see Fig. 2a). The simulated basin-averaged ice thickness was computed from the ice-covered area only for the 2003/04 ice season (Fig. 2b). The maximum domain-averaged ice thickness in late January and early February was about 9 cm, and increased to ~10.5 cm on February 17 due to a cold air outbreak on February 16. In late February, the thickness rapidly reduced to ~7.5 cm due to a warming event on February 21.

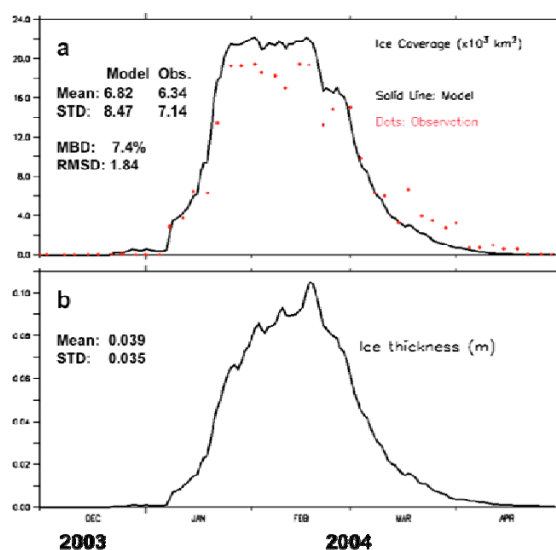


Figure 2. a) The GLIM-simulated ice area (solid, in km²) and satellite-measured ice area (dots). b) Simulated domain-averaged ice thickness (in meters) from December 1, 2003 to April 30, 2004. The simulated and observed means and standard deviations, and MBD and RMSD were provided.

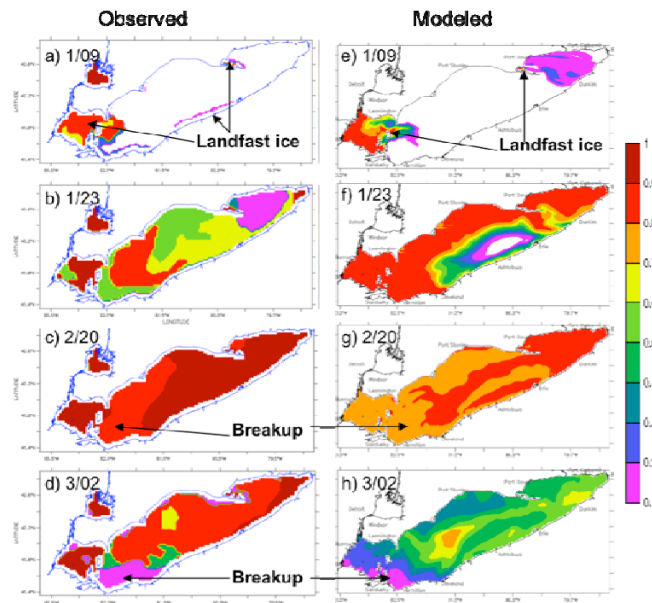


Figure 3. (Left column) Spatial distribution of the satellite-measured, 3-day composited ice concentration in 2004 on January 9 (a), and 23 (b), February 20 (c), and March 2 (d); (Right column) Same as the left column, except for the GLIM-simulated daily ice concentration.

Figure 3 shows the composite satellite-measured ice concentration during the 2003/04 ice season. On January 9, 2004, the observation shows that landfast ice formed in the western basin, while in the eastern basin, there was little ice along either the south or north shores (Fig. 3a). Ice forms more rapidly along the shores because water temperature reaches the freezing point in shallow water before it does in deeper water. On January 23, lake ice completely covered the entire lake, although with variable concentration (Fig. 3b). By January 30, Lake Erie was completely ice covered with >90% ice concentration, except for part of the eastern lake that had 70-80% ice concentration. Complete ice coverage persisted until February 20 (Fig. 3c). Lake ice started to break up in late February (not shown) along the north shore and south shore, and along the shoal-basin due to a sudden drop in water depth from 5 m to 10 m. The landfast ice west of the islands in the western lake was still 100% (Fig. 3d), because of its attachment to the shores. To the east of the islands, pack ice broke up early due to water depth (~10 m) because pack ice in deep water is more mobile than in shallow water in response to the same wind forcing. Breakup of landfast ice and pack ice near the islands is where breakup occurred first, mainly due to the discontinuity in the 10-m isobath under solar warming and wind forcing.

Figure 3 (right column) also shows the modeled spatial variability of lake ice concentration of the 2003/04 ice cycle. Landfast ice formed from the western lake and near Port Dover (Fig. 3e) because the water depth is only 5-10 m. However, the model produced more ice in the eastern lake than actual measurements showed. Lake ice expanded from the north shore to south shore on January 23 (Fig. 3f), which is a large discrepancy from observations (Fig. 3b). Breakup began in the shallow areas of the western basin in late February (Figs. 3g), and rapid melting occurred in early March (Fig. 3h), again because shallow water is heated faster by solar radiation than deep water.

The GLIM-simulated lake ice thickness superimposed with ice velocity (black arrows) and wind velocity (green arrows) for the same days of Fig. 3 are shown (Fig. 4). Seasonal variations of spatial distribution in ice thickness have similar patterns to ice concentration (Fig. 3). Landfast ice first formed in the shallow western basin on January 9 (Fig. 4a) and expanded rapidly on January 23 (Fig. 4b). Ice continued to grow from the north shore to the south shore and completely covered the whole lake on January 30. Lake ice thickness reached its maximum of about 10.5 cm on February 17 (Fig. 2b) due to a cold air outbreak, but immediately broke up and melted following an intensive warming.

Surface water circulation (black vectors) and LST (color bar), superimposed by wind velocity (green vectors), in the 2003/04 ice season are shown (Fig. 5). Surface water circulation was transient and basically wind-driven, because wind was the most vigorous forcing in the region. The surface water current was strong on the ice-free water (Fig. 5a), compared to the ice-covered water (Fig. 5b). LST distribution mimics the ice cover. On January 9, the LST dropped to freezing in the western lake, leading to the formation of landfast ice (Figs. 4a and 5a), with high LST in the deep basin in the central and eastern lake. The freezing temperatures extended from shore toward the interior (Figs. 5b). On February 20, the LST started to rise over the entire lake (Fig. 5c). LST warmed up from the west to the east (Fig. 5d), and from the coast to the interior.

3.2 Ice formation and retreat in the western, central, and eastern lake

Basin-scale lake ice formation and melting processes in the three basins (western, central, and eastern, divided by the 82.4 °W and 80.4 °W, see Fig. 1) were

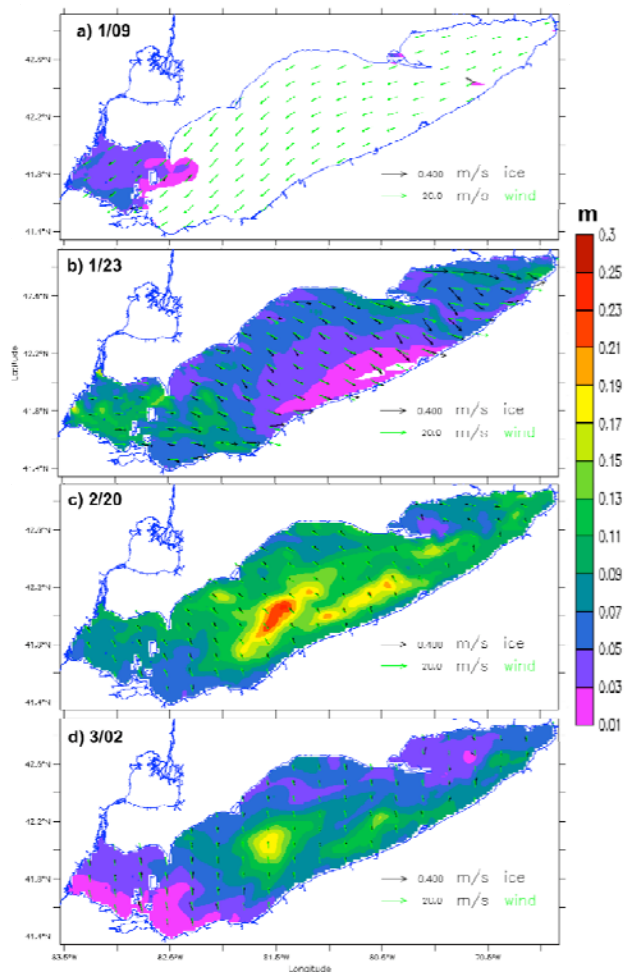


Figure 4. The GLIM-simulated daily ice thickness in 2004 on January 9 (a), and 23 (b), February 20 (c), and March 2 (d). Superimposed are the ice velocity vectors (black) and wind velocity vectors (green).

investigated. Western lake ice formed in mid December and rapidly grew, reaching a peak of 85% coverage in early February (Fig. 6a). Although ice in the central and eastern basins slowly formed in early January, ice formed rapidly in mid-January, and reached a maximum at the same time in late January as in the western basin. The high concentration persisted until late February (Fig. 6a). The decay of lake ice started from the western lake, progressed toward the central and the eastern lakes, consistent with the spatial distribution. The basin-averaged ice thickness (Fig. 6b) also shows ice thickness progression from the western to the eastern lake. The maximum ice thickness in the western basin was ~14 cm, while it was ~10.5 cm and 9 cm in the central and eastern basins, respectively.

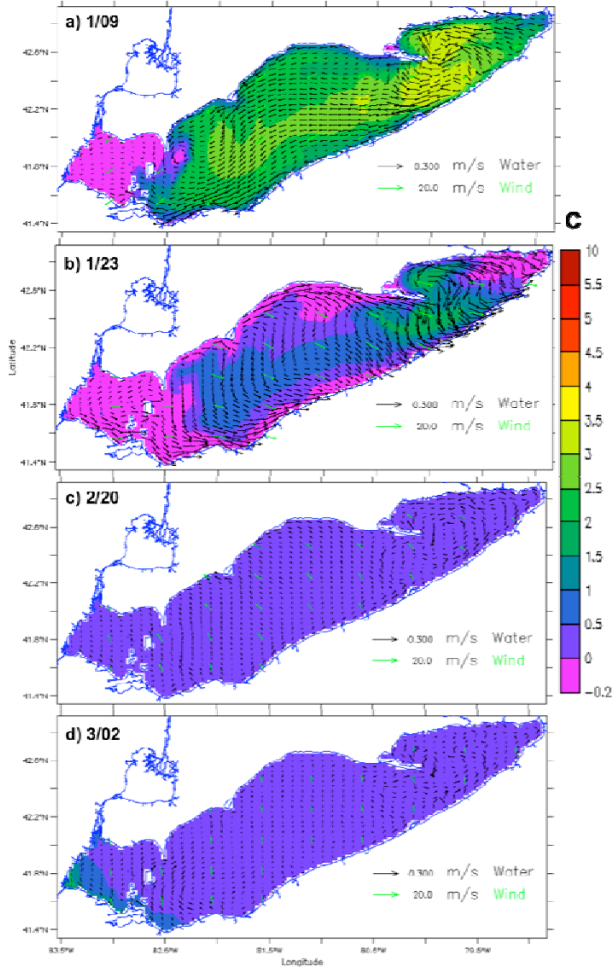


Figure 5. Same as Fig. 4, except for LST and lake surface water velocity.

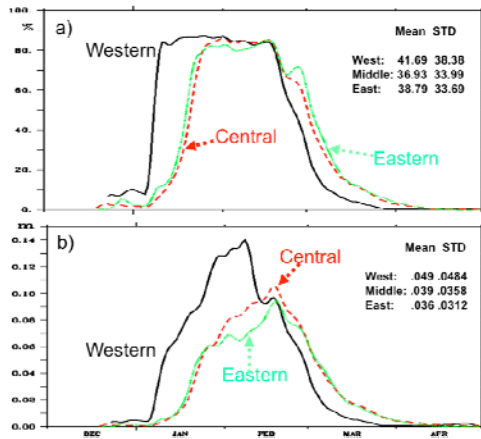


Figure 6. The GLIM-simulated basin-averaged ice concentration (a) and ice thickness (b) (in meters) from December 1, 2003 to April 30, 2004. The western lake (west of the

82.4 W line), the central lake (from 82.4W to 80.4W), and the eastern lake (east of 80.4W) are denoted by the solid/black lines, dashed/red lines, and dotted/green lines, respectively. The simulated and observed means and standard deviations were provided.

3.3 Categories of ice thickness and speed

To further examine the overall ice thickness distribution in Lake Erie, thickness histograms were constructed using the December-March simulations (Fig. 7, left column). In December, ~82% ice thickness was less than 3 cm, and ~16% ice thickness ranged from 3 to 6 cm. Only 2% of the ice thickness was over 6 cm. In January, ice moved toward thicker ice categories. In February, thick ice categories (10-20 cm and 20-30 cm) appeared. The most frequent ice thickness ranged from 3 to 10 cm, totaling 60%. In March, thin ice dominated with 89% ice being less than 3 cm, similar to December. The total (December to March) ice thickness also shows that Lake Erie is thin-ice dominant. These simulated ice thickness distributions should be validated by field measurements in the future.

A histogram based on GLIM-simulated ice speed was also constructed from December to March (Fig. 7, right column). In December, 98% of ice speeds were less than 5 cm s⁻¹ due to the nature of the landfast ice attached to shore or formed in the shallow western lake (5-10 m depth). In January, high ice speed as much as 40-60 cm s⁻¹ appeared. In February, the most frequent ice speed ranged from 5-10 cm s⁻¹ (38%) and 10-20 cm s⁻¹ (35%). In March, lake ice moved back to low speed categories with <5 cm s⁻¹ being dominant (91%), due to the reduction in wind speed. The March dominant wind is southwesterly (see Fig. 2b), which advects lake ice toward the eastern lake with small wind fetch. The total ice speeds were <5 cm s⁻¹ (64%), 5-10 cm s⁻¹ (18%), 10-20 cm s⁻¹ (4%), or 40-60 cm s⁻¹ (1%).

Campbell et al. (1987) conducted a measurement study of ice drift using four ice buoys in the central and eastern Lake Erie in winter 1983/84, which provides some useful information for our model comparison. Three of the four buoys provided ice speed values enabling us to construct a histogram for January-March 1984 (Fig. 8, upper), which compares well to the modeled total ice speed histogram (Fig. 8, lower right), except for the low speed category (<5 cm s⁻¹), because December was dominated by low ice speed. Thus, we re-construct the histogram using the simulated ice speed from January to March, 2004 only (Fig. 8, lower), the comparison is much better. This indicates that the GLIM reproduces the lake ice speed very well, although there are

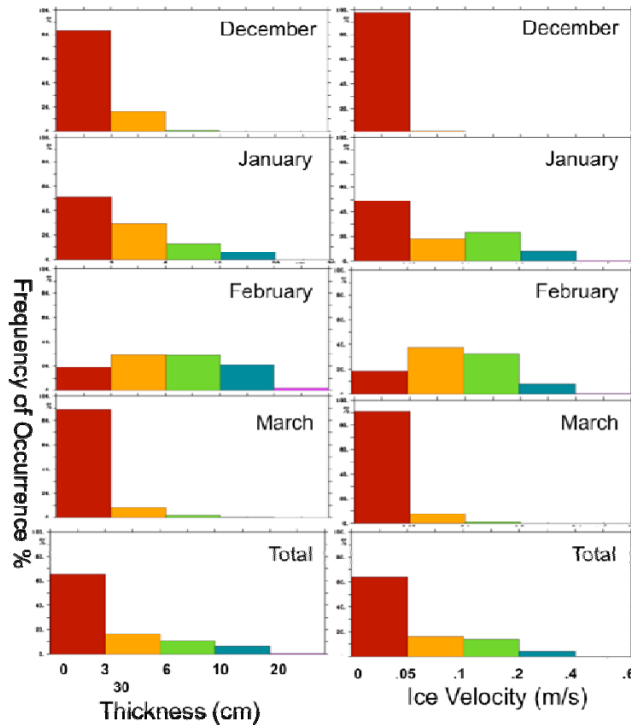


Figure 7. The histograms of the GLIM-simulated ice thickness (left column) and ice speed (right) in December, January, February, March, and the total in the 2003/04 ice season.

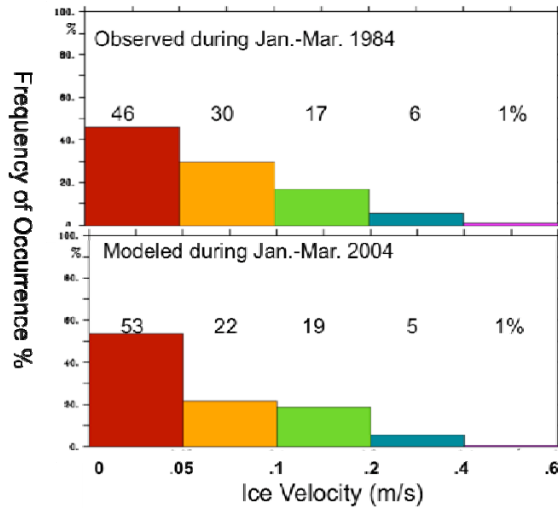


Figure 8. The histograms of observed ice drift speed during January-March, 1984 (upper; redrawn from Campbell et al. (1987)) and GLIM-simulated ice speed during January-March 2004 (lower).

differences between the model simulations and the measurements due to year-to-year variability in the wind field.

To further investigate the dynamic responses of lake ice and surface water velocities, domain- and time-averaged wind, ice velocity, and water velocity vectors were constructed at ice-covered grids only from December 2003 to April 2004 (Fig. 9). Ice drift direction is about 28 degrees to the right of the wind vector, while the surface water vector is ~17 degrees to the right of the ice drift. Therefore, the classical Ekman drift theory is still valid in an ice-covered lake, in which the surface water drift is ~45 degrees to the right of the wind vector in the northern hemisphere. In terms of magnitude, ice and surface water velocities are about 1.9% and 1.7% of the wind speed, respectively. This modifies the empirical threshold value of 2% in Lagrangian drift simulations using surface wind forcing in an ice-free ocean to 1.7% in an ice-cover lake or sea.

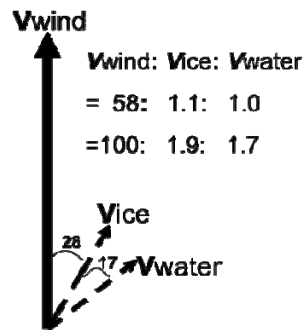


Figure 9. The domain-mean wind, ice velocity, and surface water velocity vectors versus the observed wind vector averaged from December 1, 2003 to April 30, 2004. The proportions for their magnitudes are also shown

3.4 Bi-monthly spatial variability of LST

Bi-monthly spatial distribution of LST in 2004 was simulated by the GLIM (Fig. 10, left column). February was the month with the lowest LST, with temperatures near the freezing point, indicating possible depletion of heat storage in the upper layer of the lake. Warming gradually started in March in the western lake, followed by a rapid warming from April to August. The LST in August also remained warm, but started to cool down in September. Rapid cooling occurred from October to December. In December, the cooling is from the western (shallow) to eastern (deep) lake, and from coast to basin, with visible high LST in the deep basin.

The same bi-monthly mean LST maps (Fig. 10, right column) were also constructed from the AVHRR data. The AVHRR-measured bi-monthly LST compares favorably to the modeled LST (Fig. 10) in general in other seasons, except for spring and autumn. For example, in October, the measured LST is 16-18⁰C, while the modeled LST is 15-17⁰C. The difference is ~1⁰C.

A systematic error occurred in both spring and autumn with a 1-1.5⁰C discrepancy in May and October. The most likely factor is heavy (light) cloud cover in early spring (early autumn) during the rapid warming (cooling) season. The AVHRR measurements likely underestimate (overestimate) the LST in spring (autumn) because the AVHRR composite average spans a 20-day window. As spring (autumn) progresses, the cloud cover becomes lighter (heavier), and the LST becomes warmer (colder) in spring (autumn). Thus, heavily-used images in the earlier period of the window in spring (autumn) with cloud-free (heavy cloud) conditions are heavily weighted towards the colder (warmer) conditions in early spring (early autumn), leading to the underestimate (overestimate) of LST in spring (autumn).

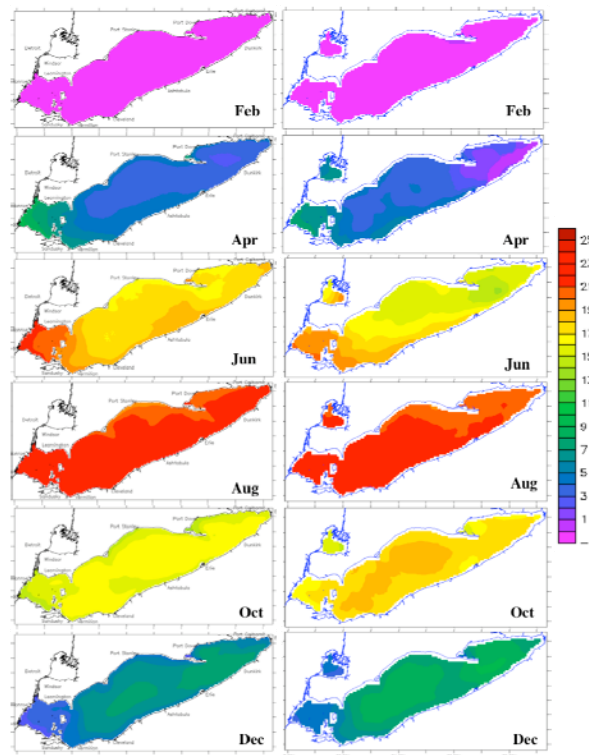


Figure 10. The GLIM-simulated monthly-averaged (left column) and AVHRR-measured monthly-averaged LST (right column) in 2004.

4. Conclusions and discussion

The Great Lakes Ice-circulation Model (GLIM) was applied to Lake Erie ice-related process studies during the 2003/04 ice season. Based on the above investigation, the following conclusions were drawn.

- 1) Lake ice formation and retreat in the western, central, and eastern lake have the following features. Lake ice forms first in the western lake and the coasts of the eastern and central lake. The ice cover in the western lake reaches a maximum ~20 days earlier than the eastern and central lake. Lake ice melts first in the western lake with a ~10-day lead. Ice completely melts in the western lake first at around the end of March, while ice in the central and eastern lake completely melts in around mid-April.
- 2) Ice thickness distribution was categorized in each month. The temporal pattern is that thin ice (<3 cm) dominates in December; thick ice gradually builds up in January, and ice thickness reaches a maximum (10-30 cm) in February. In March, lake ice is again dominated by thin ice.
- 3) Ice speed distribution has a similar temporal pattern as the ice thickness. Low ice speed (0-0.5 cm/s) dominates in December, since the landcast ice dominates. Ice speed moves to a higher values in January, reaches a maximum of 10-60 cm/s in February, and returns to low ice speed categories in March.
- 4) The GLIM-simulated ice and surface water velocity shows that the ice flows at a 28-degree angle to the right of the wind direction, while surface water flows at a 45-degree angle to the right of the wind direction. This confirms that a classical Ekman theory is valid in the ice-covered Great Lakes. The speed (magnitude) ratios of the wind to the ice surface water are 100: 1.9: 1.7, indicating that the classical rule-of-thumb of 2% between the wind and water is modified to 1.7% in an ice-covered lake or sea.

Further applications of GLIM will include: 1) update of the present GLCFS using GLIM to meet the increasing needs for winter ice forecast for safe navigation and rescue efforts, etc., 2) implementation of the ecosystem model coupled to GLIM for understanding the dynamics of lower trophic levels (e.g., phytoplankton, zooplankton), and 3) coupling GLIM to the regional climate model to accurately estimate the energy (heat and freshwater/moisture) budget over the Great Lakes.

Acknowledgments:

We sincerely thank support from NOAA GLERL for lake ice modeling research. Thanks also go to the constructive discussion with Drs. David Schwab and Marie Colton, and the satellite measurements provided by George Leshkovish. This is GLERL Contribution No. 1563.

References

- Assel, R.A., and S. Rodionov, 1998. Atmospheric teleconnections for annual maximal ice cover on the Laurentian Great Lakes. *Int. J. Climatol.*, 18, 425–442.
- Campbell, J.E., Clites, A.H., and Greene, G.M., 1987. Measurements of ice motion in Lake Erie using satellite-tracked drifter buoys. NOAA Technical Memorandum ERL GLERL-30. NOAA Great Lakes Environmental Research Laboratory, Ann Arbor, MI.
- Haapala, J., 2000. On the modelling of ice-thickness redistribution. *J. Glaciol.*, 46 (154), 427-437.
- Haapala, J., H.E.M. Meier, and J. Rinne, 2001. Numerical investigations of future ice conditions in the Baltic Sea. *Ambio*, Vol. 30, No. 4-5, 237244 (Royal Swedish Academy of Sciences).
- Hibler, W.D. III, 1979. A dynamic and thermodynamic sea ice model. *J. Phys. Oceanogr.*, 9, 15,959-15,969.
- Hibler, W.D. III, 1980. Modeling a variable thickness sea ice cover. *Mon. Wea. Rev.*, 108, 1943-1973.
- Lofgren, B.M., and P. Bieniek, 2008. Large-scale 700 hPa height patterns associated with cyclone passage and strong winds on Lake Erie. *Journal of Great Lakes Research*, 34:36-53.
- Meier, H.E.M., 2002a. Regional ocean climate simulations with a 3D ice-ocean model for the Baltic Sea. Part 1: Model experiments and results for temperature and salinity. *Climate Dyn.*, 19, 237-253.
- Meier, H.E.M., 2002b. Regional ocean climate simulations with a 3D ice-ocean model for the Baltic Sea. Part 2: Results for sea ice. *Climate Dyn.*, 19, 255-266.
- Mellor, G.L. and L. Kantha, 1989. An ice-ocean coupled model. *J. Geophys. Res.*, 94, 10,937-10,954.
- Mysak, L.A., R.G. Ingram, J. Wang, and A. van der Baaren, 1996. Anomalous sea-ice extent in Hudson Bay, Baffin Bay and the Labrador Sea during three simultaneous ENSO and NAO episodes, *Atmosphere-Ocean*, 34: 313-343.
- Saucier, F., and J. Dionne, 1998. A 3-D coupled ice-ocean model applied to Hudson

- Bay, Canada: The seasonal cycle and time-dependent climate response to atmospheric forcing and runoff, *J. Geophys. Res.*, 103(C12), 27689-27705.
- Saucier F. J., F. Roy, D. Gilbert, P. Pellerin, H. Ritchie, 2003. Modeling the formation and circulation processes of water masses and sea ice in the Gulf of St. Lawrence, Canada, *J. Geophys. Res.*, 108 (C8), 3269, doi:10.1029/2000JC000686.
- Saucier, F.J., S. Senneville, S. Prinsenber, F. Roy, G. Smith, P. Gachon, D. Caya, and R. Laprise, 2004. Modelling the sea ice-ocean seasonal cycle in Hudson Bay, Foxe Basin and Hudson Strait, Canada, *Climate Dyn.*, 23, 303-326.
- Tang, C.L., 2008. A coupled multi-category sea ice model and POM for Baffin Bay and the Labrador Sea, *Chinese J. of Polar Science*, 19 (2), 149-158.
- Thorndike, A. S., D. A. Rothrock, G. A. Maykut, and R. Colony, 1975. The thickness distribution of sea ice, *J. Geophys. Res.*, 80, 4,501-4,513
- Wake, A. and R.R. Rumer, 1979. Modeling the ice regime of Lake Erie. *J. Hydraul. Div.*, 105: 827-844.
- Wake, A. and R.R. Rumer, 1983. Great Lakes ice dynamics simulation. *J. Waterw. Port Coast. Ocean Eng.*, 109 (1): 86-1-2.
- Wang, J., L.A. Mysak and R.G. Ingram, 1994. A numerical simulation of sea-ice cover in Hudson Bay, *J. Phys. Oceanogr.*, 24, 2515-253.
- Wang, J., Q. Liu, and M. Jin, 2002. A User's Guide for a Coupled Ice-Ocean Model (CIOM) in the Pan-Arctic and North Atlantic Oceans. International Arctic Research Center-Frontier Research System for Global Change, Tech. Rep. 02-01, 65 pp.
- Wang, J., Q. Liu, M. Jin, M. Ikeda and F.J. Saucier, 2005. A coupled ice-ocean model in the pan-Arctic and the northern North Atlantic Ocean: Simulation of seasonal cycles. *J. Oceanogr.*, 61, 213-233.
- Wang, J. K. Mizobata, H. Hu, M. Jin, S. Zhang, W. Johnson, and K. Shimada, 2008, Modeling Seasonal Variations of Ocean and Sea Ice Circulation in the Beaufort and Chukchi Seas: A model-data fusion study. *Chinese Journal of Polar Science*, 19(2), 168-184.
- Wang, J., H. Hu, K. Mizobata, and S. Saitoh, 2009. Seasonal variations of sea ice and ocean circulation in the Bering Sea: A model-data fusion study. *J. Geophys. Res.*, 114, C02011, doi:10.1029/2008JC004727.
- Wang, J., H. Hu, D. Schwab, G. Leshkevich, D. Beletsky, N. Hawley and A. Clites, 2010a. Development of the Great Lakes Ice-circulation Model (GLIM): Application to Lake Erie in 2004. *Journal of Great Lakes Research* (in press)
- Wang, J., X. Bai, G. Leshkevich, M. Colton, A. Clites, and B. Lofgren, 2010b. Severe Great Lakes ice cover in winter 2008/09, *AGU EOS*, 91 (5), 41-42.

Yao, T., C.L. Tang, and I.K. Peterson, 2000. Modeling the seasonal variation of sea ice in the Labrador Sea with a coupled multi-category ice model and the Princeton Ocean Model. *J. Geophys. Res.*, 105 (C1), 1153-1165.

Table 1. Constants used in CIOM/CLIM (Note temperature is in Kelvin, $^{\circ}\text{K}$)

Symbols	Description	Values	Units
α_i	albedo of sea ice	0.28	
α_w	albedo of sea water	0.1	
C_a	wind stress bulk coef.	2.3×10^{-3}	
C_w	water stress bulk coef.	1.8×10^{-4}	
C_e	latent heat bulk transfer coef.	1.75×10^{-3}	
C_s	sensible heat bulk transfer coef.	2.32×10^{-3} when $T_s < T_a$ 1.75×10^{-3} when $T_s \geq T_a$	
C_p	specific heat of air	1410	$\text{J kg}^{-1} \text{K}^{-1}$
$C_{p,w}$	specific heat of sea water	3903	$\text{J kg}^{-1} \text{K}^{-1}$
e	yield curve eccentricity	2	
e_i	emission of sea ice	0.65-0.75	
L	volume latent heat of fusion		
L_e	latent heat sublimation on ice surface	3.32×10^{-3}	J kg^{-1}
k	von Karman constant	0.4	
k_i	thermal conductive coef.	2.04	
P^*	ice strength	$2.5 \times 10^{-4} \text{ Nm}^{-2}$	
Pr	molecular Prantl number	12.9	
ρ_a	air density	1.3	kg m^{-3}
ρ_i	sea ice density	910	kg m^{-3}
ρ_w	seawater density	1025	kg m^{-3}

S_i	ice salinity	0	psu
Sc	Schmidt number	2432	
σ	Stefan-Boltzmann constant	5.67×10^{-8}	
$\Delta x = \Delta y$	model horizontal grid size	2000	m
ΔT	time step for eternal mode	20	seconds
Δt	time step for internal mode and ice	600	seconds

